Author/s:
McMillan, M;Gleadow, A;Kohn, B;Seiler, C

Title:
Post Gondwana breakup evolution of the SE Australia rifted margin revisited

Date:
2020-04-01

Citation:
McMillan, M., Gleadow, A., Kohn, B. & Seiler, C. (2020). Post Gondwana breakup evolution of the SE Australia rifted margin revisited. Terra Nova, 32 (2), pp.109-121. https://doi.org/10.1111/ter.12441.

Persistent Link:
https://hdl.handle.net/11343/286750

DR MALCOLM MCMILLAN (Orcid ID : 0000-0002-5375-5680)
PROFESSOR BARRY KOHN (Orcid ID : 0000-0001-5064-5454)

Article type : Paper

SPECIAL ISSUE – THERMO2018

Terra Nova Draft

Title: Post Gondwana break-up evolution of the SE Australia rifted margin revisited
Short Title: Breakup evolution of SE Australia margin revisited
Footnote: This paper was presented at the 16th International Conference on Thermochronology (Quedlinburg, Germany, September 2018)

Data Availability Statement: The data that support the findings of this study are provided in the supplementary material. Any additional data including apatite fission track images and alternative file formats are available on request from the corresponding author.

Malcolm McMillan [1], Andrew Gleadow [2], Barry Kohn [3], Christian Seiler[4]
Corresponding author: McMillan, Malcolm
Email ID: malcmcm@gmail.com

[1] Address: School of Earth Sciences, The University of Melbourne, Parkville, Victoria, Australia 3010
email: m.mcmillan1@student.unimelb.edu.au
phone: +61 452 556 092
ORCID: 0000-0002-5375-5680

[2] Address: School of Earth Sciences, The University of Melbourne, Parkville, Victoria, Australia 3010
email: gleadow@unimelb.edu.au
phone: +61 383 445 700
ORCID: 0000-0003-0496-0028

[3] Address: School of Earth Sciences, The University of Melbourne, Parkville, Victoria, Australia 3010
email: b.kohn@unimelb.edu.au
phone: +61 383 447 217

ORCID: 0000-0001-5064-5454

[4]Address: School of Earth Sciences, The University of Melbourne, Parkville, Victoria, Australia 3010
email: christian.seiler@angloamerican.com
phone: +61 (0)7 3834 1001
ORCID: 0000-0002-8715-4824

Abstract

Low temperature thermochronology (LTT) is commonly used to investigate onshore records of continental rifting and geomorphic evolution of passive continental margins. The SE Australian passive margin, like many others, has an elevated plateau separated from the coastal plain by an erosional escarpment, presumed to originate through Cretaceous rifting prior to Tasman Sea seafloor spreading. Previous LTT studies have focused on reconciling thermal histories with development of the present-day topography. New apatite LTT data along an escarpment-to-coast transect define a classic 'boomerang' (mean track length vs fission-track age), indicating variable overprinting of late-Paleozoic cooling ages by a younger, mid-Cretaceous cooling event. Regionally, however, the boomerang trend diverges NNW away from the coast and crosses the escarpment, implying the underlying thermal history pre-dates escarpment formation and is largely independent from post-breakup landscape evolution. We suggest Cretaceous cooling might relate to erosion of Permo-Triassic sedimentary cover from a formerly more extensive Sydney Basin.

Introduction

Elevated passive continental margins (EPCMs) are characterized by an uplifted plateau surface separated from a broad coastal plain by one or more seaward facing erosional escarpments (e.g. Moore *et al.,* 1986; Green *et al.,* 2013; Wildman *et al.,* 2016). Such EPCMs are often persistent and are widely considered to contain important records of continental breakup and subsequent margin denudation (e.g. Kollenz *et al.,* 2016; Hueck *et al.,* 2019). Interpretation of these margins has been controversial, however, with various conceptual models proposed to explain their development (e.g. Lister *et al.,* 1986; Gilchrist and Summerfield 1990; Gilchrist *et al.,* 1994; Kooi and Beaumont, 1994; Gallagher and Brown, 1997; Braun and van der Beek, 2004). Low-temperature thermochronology (LTT) using apatite fission-track (AFT) and apatite (U-Th-Sm)/He (AHe) methods (e.g. Gleadow *et al.,* 2002a; Reiners *et al.,* 2018), has commonly been used to constrain the onshore development of EPCMs (see Wildman *et al.,* 2019 for overview), starting with the classic study of Moore *et al.* (1986) on the SE Australia margin.

Following recognition by Gleadow and Lovering (1978) of a possible association between AFT ages and continental rifting, Moore (1982) conducted the first regional AFT thermochronology study of the SE Australia EPCM, dominated by the "Great Escarpment" (e.g. Ollier, 1982; Braun & van der Beek, 2004; Heimsath & Chappell 2006), the significance of which has featured in many subsequent studies (e.g. Moore *et al.,* 1986; Dumitru *et al.,* 1991;

O'Sullivan *et al.,* 1995; van der Beek *et al.,* 1999; Kohn *et al.,* 2002; Persano *et al.,* 2002). All of these studies have implicitly assumed a relationship between the evolution of the present topography and the underlying thermochronology, which has recently been called into question by Green *et al.* (2013, 2018). Central to this margin is an E-W transect from the Monaro Tableland across the Brown Mountain escarpment to the coast. However, published AFT data from this area, mostly from Moore (1982) and Moore *et al.* (1986), pre-date many important developments in methodology, interpretation and modeling (e.g. Green 1986; Donelick *et al.,* 2005; Ketcham *et al.,* 2007b; Gleadow *et al.,* 2009; Gallagher, 2012;). Moreover, ideas on the geomorphic and geological development of rifted margins have also evolved (e.g. Gallagher *et al.,* 1998; Braun and van der Beek, 2004; Braun, 2018a, 2018b; Green *et al.,* 2013, 2018; Japsen *et al.,* 2018).

Moore *et al.* (1986) suggested a thermal event associated with rifting may have preferentially reset AFT ages along the margin, with diminishing effect inland, leaving undisturbed Paleozoic cooling ages on the elevated plateau. The LTT data were thought to represent a pattern of increasing denudation and/or increasing heat flow towards the coast, discussed in a number of subsequent studies (e.g. Dumitru *et al.,* 1991; O'Sullivan *et al.,* 1995; van der Beek *et al.,* 1999; Persano *et al.,* 2002, 2005). The term "boomerang trend" was coined to describe a concave-up trend of AFT age against mean track length, first observed by Moore (1982) and explained more fully by Green (1986), resulting from progressive overprinting of an older background age by a younger cooling event.

One explanation for the observed LTT data pattern is variable denudation across the coastal plain (<2km at escarpment to >4km at coast) using a constant geothermal gradient (~25°C/km). This requires significant vertical displacement by faulting or very low lithospheric rigidity (effective elastic thickness (EET) ~5-8km, Braun and van der Beek, 2004). Evidence for substantial faulting or flexure is lacking in the field area and within the generally flat-lying Permo-Triassic Sydney Basin to the north (Middleton and Schmidt, 1982; Moore *et al.,* 1986; Persano *et al.,* 2005). Furthermore, gravimetric and heat flow studies along eastern Australia suggest a minimum EET of ~15km (e.g. Zuber *et al.,* 1989; Simons *et al.,* 2000). Some studies have therefore proposed heating associated with rifting might decrease the km-scale denudation required (Moore *et al.*, 1986; Persano *et al.,* 2005).

Over the last 20 years, prevailing explanations for LTT trends along rifted margins have mostly favored denudation mechanisms associated with escarpment formation. The SE Australian margin has generally been thought to follow 'scarp retreat' or 'pinned-divide' models (e.g. Gilchrist and Summerfield, 1990; Gallagher *et al.,* 1998; Persano *et al.,* 2002, 2005), aided by stream incision seaward of the drainage divide (Heimsath and Chappell, 2006; van der Beek and Braun, 2002). Distinguishing between these two scenarios is difficult (Braun and van der Beek, 2004), but LTT data are generally regarded as inconsistent with a down-warped model (e.g. Ollier and Pain, 1997). Periods of most rapid erosion have been linked to early stages of rifting and seafloor spreading (Matmon *et al.,* 2002, Persano *et al.,* 2005). This is supported by the presence of Eocene basalts (~55-35 Ma, Wellman and McDougall, 1974; Matchan, 2012) on the Monaro Tableland and parts of the escarpment, implying that relief developed by the late Cretaceous with minimal erosion and no significant uplift of the Monaro since that time (e.g. Taylor *et al.,* 1985, 1990; McQueen, 1994; Bishop and Goldrick, 1997; van der Beek and Braun, 1998). In contrast, Green *et al.* (2013, 2018) suggest that most uplift and escarpment formation considerably post-date rifting (Oligocene-present).

In this study, we revisit the classic Brown Mountain transect in SE Australia and present a new LTT data set utilizing modern AFT analytical techniques, complemented by AHe data and thermal history modelling. These are then compared with regional data sets to provide further insights into the thermal and geomorphic evolution of the margin.

Geologic Setting

The erosional escarpment along the EPCM of SE Australia runs ~50-200km inland and roughly parallel to the coast separating the relatively high (up to 1300m) Monaro Tableland to the west, from a low-lying coastal plain to the east (Ollier, 1982, 1985; Wellman, 1987). The margin resulted from the break-up of eastern Gondwana and separation of the continental Lord Howe Rise by opening of the Tasman Sea. Rifting commenced ~110-90Ma (Jones and Veevers, 1983) with seafloor spreading occurring between ~74-52Ma (Gaina *et al*., 1998). Local geology (Figure 1) consists of Silurian-Devonian granitoids intruding early Paleozoic sediments of the Lachlan Fold Belt (e.g. Foster and Gray, 2000). The Permo-Triassic Sydney Basin (e.g. Middleton and Schmidt, 1982) occurs ~140km north of the study area. Several small Cretaceous and Jurassic intrusions occur along the SE margin. The small (~5km^2) Cretaceous Tanja Syenite outcrops along the transect (~3km inland) and the 99Ma Mt. Dromedary Complex (Schoene *et al.,* 2006; Phillips *et al.,* 2017) outcrops ~60km north of the study area.

Sampling, Methods and Results

Samples were collected along a transect from the Monaro Tableland to the coast (Figure 1). AFT and AHe analytical methods follow Gleadow *et al.* (2015) with results presented in Tables 1 and 2, respectively and Figure 2. AFT results are grouped into 3 zones (Figures 1 & 2) representing distinct sets based on age and track-length distributions. In general, AFT ages decrease from a maximum of ~290Ma above the escarpment, to a minimum of ~70-90Ma at the coast. Longer mean track lengths (MTL) are found at each end of the transect, with shorter MTL between. AHe central ages (used for non-dispersed age samples; Vermeesch, 2008) follow this same general trend, with a minimum (~80Ma) near the coast and maximum (~135Ma) at the top of the escarpment.

Zone 1 samples (AFT ages >250Ma) exhibit narrow unimodal track-length distributions (Figure 2) with the longest furthest from the coast at 13.2±0.7µm (MM14-01). Zone 2 samples (intermediate AFT ages from 239±12Ma to 139±6Ma) yield negatively skewed or bimodal track-length distributions with MTL ranging from 12.2±1.9 to 9.6±2.6µm. Clearly bimodal distributions occur ~25-15km from the coast. Zone 3 samples (AFT ages 114±9Ma to 73±4Ma) yield longest MTL, averaging ~13.8±1µm with narrow unimodal length distributions. Two younger ages, 37±11Ma (MM14-22) and 71±28Ma (MM14-23), show highly dispersed single grain ages (see Supplementary Information), and are possibly affected by forest fire.

Most AHe data show only minor intra-sample age dispersion, although in some (MM14-13, 24) dispersion is excessive and these results were not used in thermal history modeling. The oldest AHe central age is 131±6Ma (MM14-5), at the top of the escarpment, and ages gradually decrease to 85±3Ma and 93±3Ma towards the coast. A similar AHe age pattern (with some age dispersion) was also reported by Persano *et al.* (2002) (see Figures 2 and 3),.

Discussion

The relationship between MTL and apparent AFT age (Figure 4) shows a classic concave-up 'boomerang' trend, (e.g. Moore *et al.,* 1982, 1986**;** Green, 1986) implying that variation in apparent ages is controlled by a mixture of two distinct cooling events in differing proportions. The boomerang trend across the coastal plain is summarized in Figure 3. The overall trend is similar to that of Moore *et al.* (1986), but here the 'trough' is more pronounced, down to ~10µm

MTL compared to at least 1μm greater in the same area, probably due to the measurement of anomalously long TINCLE tracks (Donelick *et al*., 2005).

Zone 3 MTL and younger ages suggest rapid mid-Cretaceous (~90Ma) cooling (broadly coinciding with the onset of rifting), the effect of which diminishes inland.. Zone 2 samples possess broader and/or bimodal track length distributions representing two distinct age components. The shortening and progressive loss of the older, and increasing presence of the younger, component towards the coast results in the boomerang trend trough observed in Zone 2.

The concave-up boomerang trend with distinct end-member cooling components, seemingly associated with escarpment topography, has been used as evidence to reconcile highly variable denudation along the coastal plain. However, regional AFT studies (Kohn *et al.,* 2002; Gleadow *et al.* 2002b) show the boomerang trough continues northwards and diverges inland (Figure 5), crossing both the escarpment and the elevated plateau. This implies the regional AFT pattern must pre-date the denudation history represented by escarpment retreat, suggesting the apparent relationship between the two in the study area may be fortuitous. Furthermore, the areas of coastal resetting (MTL ~14μm) and the trend of the boomerang trough, closely parallels the present edge of Sydney Basin (Figure 5) suggesting it may have previously extended significantly to the west and south blanketing the area. Erosional removal of this sedimentary cover would have contributed to the underlying thermal history and, as argued by Green *et al.* (2013, 2018), pre-dated formation of the escarpment.

Inverse thermal history models are summarized in Figure 6 and Supplementary Information. Zone 1 sample MM14-05 shows fairly rapid late-Paleozoic cooling to relatively low temperatures, possibly followed by mild Neogene cooling. Zone 3 samples show rapid cooling at ~90Ma from temperatures (>~120°C), above the apatite partial annealing zone (PAZ), followed by rapid cooling to the surface within ~15-25Myr. Sample MM14-20 from the sub-volcanic Cretaceous Tanja Syenite (99Ma, in prep.), one of several regional Cretaceous and Jurassic intrusions (Lewis *et al.,* 1994), is similar in age to the nearby Mt. Dromedary intrusion. Within uncertainty, the AFT age (and long MTL) is consistent with the emplacement age, suggesting Tanja has not experienced prolonged exposure in the PAZ since emplacement. Nott and Purvis (1995) argued that the escarpment already lay to the west of Mt. Dromedary by the mid-Cretaceous. Similarly here, the Tanja syenite and late-Cretaceous coastal ages are consistent with models of rapid escarpment migration in the early stages of rifting (Matmon *et al.,* 2002; Persano *et al.,* 2005).

Modeling results for Zone 2 suggest at least minor reheating during the early-mid Cretaceous, but due to partial annealing of older/shorter tracks, evidence for this phase is absent in Zone 3. Forward models based on broadly similar data sets (Persano *et al*., 2005), do not show this reheating and instead exhibit longer residence within the AFT and AHe partial retention zones. It is not clear whether those models allowed for reheating or were cooling-only, but clearly either strategy will produce acceptable results and such reheating is permitted, rather than demanded by the data.

Timing of the thermal maximum apparent in Zones 2 and 3 prior to rapid cooling, approximately coincides with emplacement of the Tanja Syenite. Such relatively small intrusions would likely have little regional thermal effect, but might be associated with elevated thermal gradients, if combined with a more extensive low-conductivity sedimentary blanket. In the southern Sydney Basin, ~140km to the north, Schmidt and Embleton (1981) and Middleton and Schmidt (1982) found evidence for a substantial Cretaceous paleomagnetic overprint affecting the coastal areas at ~100-70Ma, coinciding with very high vitrinite reflectance values, together indicating paleotemperatures of ~200°C.

These findings were interpreted as resulting from high thermal gradients (up to 70°C/km) under km-scale cover followed by rapid mid Cretaceous exhumation and cooling. A higher geothermal gradient in the study area would reduce the total exhumation required, thereby allowing for a greater, more reasonable effective elastic thickness (~60°C/km equates to ~1.4km of exhumation and an ETT of ~10km; see Table 3).

The data presented here confirm that large-scale variable denudation or elevated thermal gradients are required to explain the observed LTT trends. The regional AFT pattern implies that denudation related to escarpment retreat or heating associated with rifting alone cannot fully explain the findings. We suggest the Sydney Basin may have extended further southwest than previously thought, allowing for higher temperatures beneath a more extensive sedimentary blanket. The boomerang trend must have existed before escarpment formation and therefore would only have been modified to a small degree by escarpment retreat. This re-interpretation may have important implications for studies that rely on similar LTT trends elsewhere and their assumed genetic relationship to escarpment denudation.

Conclusions

This study reports new LTT data and inverse time-temperature modeling for the SE Australian rifted margin and compares these with regional thermochronology trends. The results constrain the regional thermal history and confirm rapid cooling in coastal areas at ~90Ma. This event overlaps with the time of rifting prior to the onset of seafloor spreading in the adjacent Tasman Sea. Models for samples with bimodal track length distributions from the middle of a classic boomerang-trend of MTL against AFT age are consistent with a rise in geothermal gradient around this time. The divergent NNW path of the boomerang trend away from the coast suggests the LTT pattern must pre-date formation of the erosional escarpment. Based on the relationship of this trend to the Sydney Basin, we suggest that basin sediments may have extended across the study area prior to rapid Cretaceous cooling, thus mitigating the requirement for km-scale denudation.

Acknowledgements

The Melbourne thermochronology laboratory receives support under the AuScope program of the Australian National Collaborative Research Infrastructure Strategy (NCRIS). This study was supported by an Australian Research Council Discovery grant (DP 1092861). Abaz Alimanović provided technical assistance with (U-Th)/He analyses. Samuel Boone is thanked for providing field assistance. The authors have no conflict of interest to declare.

References

Bishop, P. and Goldrick, G., 1997. Eastern Australia. In: *Global tectonics and geomorphology.* John Wiley, New York.

Braun, J., and van der Beek, P., 2004. Evolution of passive margin escarpments: What can we learn from low-temperature thermochronology? *Journal of Geophysical Research*, **109**.

Braun, J., 2018a. A review of numerical modeling studies of passive margin escarpments leading to a new analytical expression for the rate of escarpment migration velocity. *Gondwana Research*, **53,** 209-224.

Braun, J., 2018b. Response to comment by Japsen et al. on "A review of numerical modeling studies of passive margin escarpments leading to a new analytical expression for the rate of escarpment migration velocity". *Gondwana Research*.

Brown, R., 1991. Backstacking apatite fission-track stratigraphy: A method for resolving the erosional and isostatic rebound components of tectonic uplift histories. *Geology*, **19**, 74-77.

Donelick, R. A., O'Sullivan, P. B. and Ketcham, R. A., 2005. Apatite fission-track analysis. *Reviews in Mineralogy and Geochemistry*, **58,** 49-94.

Dumitru, T. A., Hill, K. C., Coyle, D. A., Duddy, I. R., Foster, D. A., Gleadow, A. J. W., Green, P. F., Kohn, B. P., Laslett, G. M. and O'Sullivan, P. B., 1991. Fission track thermochronology: Application to continental rifting of southeastern Australia. *Australian Petroleum Exploration Association*, **31,** 131-142.

Farley, K. A., Wolf, R. A. and Silver, L. T., 1996. The effects of long alpha-stopping distances on (U-Th)/He ages. *Geochimica et Cosmochimica Acta*, **60,** 4223-4229.

Foster, D. A. and Gray, D. R., 2000. Evolution and Structure of the Lachlan Fold Belt (Orogen) of Eastern Australia. *Annual Review of Earth and Planetary Science*, **28,** 47-80.

Gaina, C., Müller, R.D., Rover, J.-Y., Stock, J., Hardebeck, J., Symonds, P., 1998. The tectonic history of the Tasman Sea: a puzzle with 13 pieces. *Journal of Geophysical Research* 103, 12413-12433.

Galbraith, R. F., 2005. *Statistics for fission track analysis*. Chapman and Hall/CRC Press.

Gallagher, K. and Brown, R. W., 1997. The onshore record of passive margin evolution. *Journal of the Geological Society*, **154,** 451-457.

Gallagher, K., Brown, R. W. and Johnson, C., 1998. Fission track analysis and its applications to geological problems. *Annual Review of Earth and Planetary Science*, **26,** 519-572.

Gallagher, K., 2012. Transdimensional inverse thermal history modeling for quantitative thermochronology. *Journal of Geophysical Research: Solid Earth*, **117**.

Gilchrist, A. R. and Summerfield, M. A., 1990. Differential denudation and flexural isostasy in formation of rifted-margin upwards. *Nature*, **346,** 739-742.

Gilchrist, A. R., Kooi, H. and Beaumont, C., 1994. Post-Gondwana geomorphic evolution of southwestern Africa: Implications for the controls on landscape development from observations and numerical experiments. *Journal of Geophysical Research: Solid Earth,* **99,** 12211-12228.

Gleadow, A. J. W. and Lovering, J.F., 1978. Fission track geochronology of King Island, Bass Strait, Australia: relationship to continental rifting. *Earth and Planetary Science Letters,* **37**, 429-437.

Gleadow, A. J. W., Belton, D., Kohn, B. P. and Brown, R. W., 2002a. Fission Track Dating of Phosphate Minerals and the Thermochronology of Apatite. *Reviews in Mineralogy and Geochemistry*, **48**, 579-630.

Gleadow, A. J. W., Kohn, B. P., Brown, R. W., O'Sullivan, P. B. and Raza, A., 2002b. Fission track thermotectonic imaging of the Australian continent. *Tectonophysics*, **349**, 5-21.

Gleadow, A. J. W., Gleadow, S. J., Belton, D. X., Kohn, B. P., Krochmal, M. S. and Brown, R. W., 2009. Coincidence mapping – a key strategy for the automatic counting of fission tracks in natural minerals. *Thermochronological Methods: From Palaeotemperature Constraints to Landscape Evolution Models,* **324,** 25-36.

Gleadow, A. J. W., Harrison, M., Kohn, B. P., Lugo-Zazueta, R. and Phillips, D., 2015. Fish Canyon Tuff apatite: A new look at an old low-temperature thermochronology standard. *Earth and Planetary Science Letters*, **424**, 95-108.

Green, P. F., 1986. On the thermo-tectonic evolution of Northern England: evidence from fission track analysis. *Geological Magazine*, **123,** 493-506.

Green, P.F., 1988. The relationship between track shortening and fission track age reduction in apatite: combined influences of inherent instability, annealing anisotropy, length bias and system calibration. *Earth and Planetary Science Letters*, **89**, 335-352.

Green, P. F., Lidmar-bergström, K., Japsen, P., Bonow, J. M. and Chalmers, J. A., 2013. Stratigraphic landscape analysis, thermochronology and the episodic development of elevated passive continental margins. *Geological Survey of Denmark and Greenland,* **30**, 150pp.

Green, P. F., Japsen, P., Chalmers, J. A., Bonow, J. M. and Duddy, I. R., 2018. Post-breakup burial and exhumation of passive continental margins: Seven propositions to inform geodynamic models. *Gondwana Research*, **53**, 58-81.

Hasebe, N., Barbarand, J., Jarvis, K., Carter, A., and Hurford, A. J., 2004. Apatite fission-track chronometry using laser ablation ICP-MS. *Chemical Geology.* **207,** 135-145.

Hayes, D. E. and Ringis, J., 1973. Seafloor spreading in the Tasman sea. *Nature*, **243,** 454-458.

Heimsath, A. and Chappell, J., 2006. Escarpment erosion and landscape evolution in southeastern Australia. *Geological Society of America*, **398,** 173-190.

Hueck, M., Dunkl, I., Oriolo, S., Wemmer, K., Basei, M.A. and Siegesmund, S., 2019. Comparing contiguous high- and low-elevation continental margins: New (U-Th)/He constraints from South Brazil and an integration of the thermochronological record of the southeastern passive margin of South America. *Tectonophysics*, 228222.

Japsen, P., Green, P. F., Chalmers, J. A., Duddy, I., and Bonow, J. M., 2018. Elevated passive continental margins: Numerical modeling vs observations. A comment on Braun (2018). *Gondwana Research,* **65**, 172-173.

Jiao, R., Seward, D., Little, T. A. and Kohn, B. P., 2014. Thermal history and exhumation of basement rocks from Mesozoic to Cenozoic subduction cycles, central North Island, New Zealand. *Tectonics*, **33**, 1920-1935.

Jones, J., and Veevers, J., 1983. Mesozoic origins and antecedents of Australia's Eastern highlands. *Journal of the Geological Society of Australia,* **30,** 305-321.

Ketcham, R. A., 2005. Forward and Inverse Modeling of Low-Temperature Thermochronometry Data. *Reviews in Mineralogy and Geochemistry*, **58**, 275-314.

Ketcham, R. A., Carter, A., Donelick, R. A., Barbarand, J. and Hurford, A. J., 2007a. Improved measurement of fission-track annealing in apatite using c-axis projection. *American Mineralogist*, **92**, 789-798.

Ketcham, R. A., Carter, A., Donelick, R. A., Barbarand, J. and Hurford, A. J., 2007b. Improved modeling of fission-track annealing in apatite. *American Mineralogist*, **92**, 799-810.

Kohn, B. P., Gleadow, A. J. W., Brown, R. W., Gallagher, K., O'Sullivan, P. B. and Foster, D. A., 2002. Shaping the Australian crust over the last 300 million years: Insights from fission track thermotectonic imaging and denudation studies of key terranes. *Australian Journal of Earth Sciences*, **49**, 697-717.

Kohn, B. P., Chung, L. and Gleadow, A. J. W., 2019. Fission-Track Analysis: Field Collection, Sample Preparation and Data Acquisition. In: M.G. Malusa and P.G. Fitzgerald (eds), *Fission track thermochronology and its application to geology*. Springer-Nature. 373-393.

Kollenz, S., Glasmacher, U.A., Rossello, E.A., Stockli, D.F., Schad, S. and Pereyra, R.E., 2017. Thermochronological constraints on the Cambrian to recent geological evolution of the Argentina passive continental margin. *Tectonophysics*, **716**, 182-203.

Kooi, H. and Beaumont, C., 1994. Escarpment evolution on high-elevation rifted margins: Insights derived from a surface processes model that combines diffusion, advection, and reaction. *Journal of Geophysical Research: Solid Earth,* **99,** 12191-12209.

Lewis, P., Glen, R., Pratt, G. and Clarke, I., 1994. Unpubl. Map. *Bega-Mallacoota 1:250 000 Geological Sheet*

Sj/55-4, SJ/55-8: Explanatory Notes. Geological survey of New South Wales.

Lister, G. S., Etheridge, M. A. and Symonds, P. A., 1986. Detachment faulting and the evolution of passive continental margins. *Geology*, **14**, 246-250.

Matchan, E. L., 2012. Calibration of the cosmogenic 21Ne exposure dating technique for application to Quaternary volcanic chronology. Unpubl. doctoral dissertation, University of Melbourne, Melbourne, Australia.

Matmon, A., Bierman, P. and Enzel, Y., 2002. Pattern and tempo of great escarpment erosion. *Geology*, **30,** 1135-1138.

McQueen, K. G., 1994. Consensus on the Monaro? Directions for future research. *Conference proceedings.*

Middleton, M. F. and Schmidt, P. W., 1982. Paleothermometry of the Sydney Basin. *Journal of Geophysical Research*, **87,** 5351-5359.

Moore, M. E., 1982. Thermotectonic evolution of southeastern Australia: an apatite fission track dating study. Unpubl. doctoral dissertation, The University of Melbourne, Melbourne, Australia, 346pp.

Moore, M. E., Gleadow, A. J. W. and Lovering, J. F., 1986. Thermal evolution of rifted continental margins: new evidence from fission tracks in basement apatites from southeastern Australia. *Earth and Planetary Science Letters*, **78,** 255-270.

Nott, J. and Purvis, A. C., 1995. Geomorphic and tectonic significance of early Cretaceous lavas on the coastal plain, southern New South Wales. *Australian Journal of Earth Sciences*, **42**, 145–149.

Ollier, C. D., 1982. The great escarpment of eastern Australia: tectonic and geomorphic significance. *Journal of the Geological Society of Australia*, **29,** 13-23.

Ollier, C. D., 1985. Morphotectonics of passive continental margins: Introduction. *Geomorphology*, **54,** 1-9.

Ollier, C. D. and Pain, C. F., 1997. Equating the basal unconformity with the palaeoplain: A model for passive margins. *Geomorphology*, **19,** 1-15.

O'Sullivan, P.B., Foster, D. A., Kohn, B. P., Gleadow, A. J. W. and Raza, A., 1995. Constraints on the dynamics of rifting and denudation on the eastern margin of Australia: fission track evidence for two discrete causes of rock cooling: In Proc. *Pacific Rim Conference,* 441-446.

Persano, C., Stuart, F. M., Bishop, P. and Barfod, D. N., 2002. Apatite (U-Th)/He age constraints on the development of the Great Escarpment on the southeastern Australian passive margin. *Earth and Planetary Science Letters*, **200,** 79-90.

Persano, C., Stuart, F. M., Bishop, P. and Dempster, T. J., 2005. Deciphering continental breakup in eastern Australia using low- temperature thermochronometers. *Journal of Geophysical Research: Solid Earth*, **110,** 1-17.

Phillips, D., Matchan, E.L., Honda, M. and Kuiper, K.F., 2017. Astronomical calibration of 40Ar/39Ar reference minerals using high-precision, multi-collector (ARGUSVI) mass spectrometry. *Geochimica et Cosmochimica Acta*, **196**, 351-369.

Reiners, P. W., Carlson, R. W., Renne, P. R., Cooper, K. M., Granger, D. E., McLean, N. M. and Schoene, B., 2018. Ch. 11 The (U-Th)/He system. In: *Geochronology and Thermochronology.* John Wiley & Sons Ltd, Hoboken, N. J.

Schmidt, P. W. and Embleton B. J. J., 1981. Magnetic overprinting in southeastern Australia and the thermal history of its rifted margins. *Journal of Geophysical Research*, **86**, 3998-4008.

Schoene, B., Crowley, J.L., Condon, D.J., Schmitz, M.D. and Bowring, S.A., 2006. Reassessing the uranium decay constants for geochronology using ID-TIMS U–Pb data. *Geochimica et Cosmochimica Acta*, **70**, 426-445.

Seiler, C., Kohn, B. P. and Gleadow, A. J. W., 2014. Apatite fission track analysis by LA-ICP-MS: An evaluation of the

absolute dating approach. *International conference on thermochronology*.

Simons, J. F., Maria, T. Z., Jun, K., 2000. Isostatic response of the Australian lithosphere: Estimation of effective elastic thickness and anisotropy using multitaper spectral analysis. *Journal of Geophysical Research*, **105,** 163-184.

Taylor, G. R., Bink, M., Foudoulis, C., Gordon, I., Hedstrom, J., Minello, J. and Whippy, F., 1985. Pre-basaltic topography of the Northern Monaro and its implications. *Australian Journal of Earth Sciences*, **32**, 65-71.

Taylor, G., Truswell, E. M., McQueen, K. G. and Brown, M. C., 1990. Early Tertiary palaeogeography, landform evolution, and palaeoclimates of the Southern Monaro, N.S.W., Australia. *Palaeogeography, Palaeoclimatology, Palaeoecology*, **78**, 109-134.

Turcotte, D.L. and Schubert, G., 1982. Geodynamics: Applications of continuum physics to geological problems. John Wiley, Hoboken, N. J.

Turcotte, D.L., 1979. Flexure. *Advances in Geophysics*, **21**, 51-86.

van der Beek, P. and Braun, J., 1998. Numerical modelling of landscape evolution on geological time-scales: a parameter analysis and comparison with the south-eastern highlands of Australia. *Basin Research*, **10**, 49-68.

van der Beek, P. A., Braun, J. and Lambeck, K., 1999. Post-Palaeozoic uplift history of southeastern Australia revisited: results from a process-based model of landscape evolution. *Australian Journal of Earth Sciences,* **46**, 157-172.

van der Beek, P. A. and Braun, J., 2002. Controls on post-mid-Cretaceous landscape evolution in the southeastern highlands of Australia: Insights from numerical surface process models. *Journal of Geophysical Research: Solid Earth,* **104,** 4945-4966.

Vermeesch, P., 2008. Three new ways to calculate average (U-Th)/He ages. *Chemical Geology*, **249**, 339-347.

Walcott, R.I., 1970. Flexural rigidity, thickness, and viscosity of the lithosphere. *Journal of Geophysical Research*, **75**, 3941-3954.

Weissel, J. K. and Hayes, D. E., 1977. Evolution of the Tasman Sea reappraised. *Earth and Planetary Science Letters*, **36,** 77-84.

Wellman, P., McDougall, I., 1974. Potassium-argon ages on the Cainozoic volcanic rocks of New South Wales. *Journal of the Geological Society of Australia*, **21**, 242-272.

Wellman, P., 1987. Eastern highlands of Australia; their uplift and erosion. *Journal of Australian Geology & Geophysics*, **10**, 277-286.

Wildman, M., Brown, R., Beucher, R., Persano, C., Stuart, F., Gallagher, K., Schwanethal, J. and Carter, A., 2016. The chronology and tectonic style of landscape evolution along the elevated Atlantic continental margin of South Africa resolved by joint apatite fission track and (U-Th-Sm)/He thermochronology. *Tectonics*, **35**, 511-545.

Wildman, M., Cogné, N. and Beucher, R., 2019. Fission-track thermochronology applied to the evolution of passive continental margins. In: *Fission-Track Thermochronology and its Application to Geology*, Springer, Cham, 351-371.

Zuber, M. T., Bechtel, T. D. and Forsyth, D. W., 1989. Effective elastic thicknesses of the lithosphere and mechanisms of isostatic compensation in Australia. *Journal of Geophysical Research: Solid Earth*, **94,** 9353-9367.

Figure Captions

Figure 1: DEM and geological map showing location of twenty-six new samples (white dots) collected on a trend perpendicular to the coast along the SE margin of NSW, Australia, near the town of Bega and Tathra following previous work in the area (Moore et al., 1986; Dumitru et al., 1991; Kohn et al., 2002; Persano et al., 2002; Persano et al., 2005). AHe samples from Persano et al., (2002) referred to in the text are marked with grey triangles. Sample elevations range from 1130 m (Samples MM14-2) to <10 m. Most samples were I-type granites except for samples MM14-22, 23 (A-type) samples 17 and 21 (Ordovician Sandstones) and MM14-20 (Cretaceous Tanja syenite).

Figure 2: AFT age and track length results along coastal transect showing histograms with kernel density estimation—blue line (y-axis = relative abundance, x-axis = length (μm) from 0-20 μm) filled with respect to their zone (zone 1 – green, zone 2 – grey, zone 3 – black). Zone 1 includes samples above the escarpment at high elevations to the west of the escarpment lip, Zone 2 includes intermediate mixing ages with bimodal MTL distributions along the escarpment and much of the coastal plain and Zone 3 includes samples along the coast with long MTLs and younger AFT ages. AFT ages (Ma) ± 1σ are marked in **bold**. MTL appears below AFT age as *italics*. AHe age (when measured) appears in parenthesis. Persano et al., (2002) AHe ages (average-Ma), referred to in the text, are marked grey.

Figure 3: Cross-section A-A' with 10x vertical exaggeration. AFT age trend is represented by the contour colors (upper plot). The lower plot shows the low-T data trends. Sample near the coast with AFT age 85±7 Ma and AHe age 93±3 Ma is a combined projected location of coastal samples MM14-21 and MM14-18B respectively. AHe ages follow the same general trend as AFT ages, where older ages belong to those rocks along the escarpment. Based on the LTT age trend along the coastal plain and inland location of age minima, the data support an escarpment retreat or down-wearing models as suggested in previous studies (Persano et al., 2002; Persano et al., 2005). Considering the probable high erosional rate of the escarpment, differentiating between these two proposed models would be difficult (Braun and van der Beek, 2004).

Figure 4: Boomerang plot, showing time period of rifting (green block) and concave-up trend (blue curve). Note: The x-axis has been flipped to relate the trend in ages with those seen along transect A-A` when moving west to east. Coastal samples (right side) show the longest MTLs and youngest AFT ages, anchoring one end member of the boomerang. Older samples near the escarpment edge (left side) with long MTLs, anchor the other end member. 'Valley' samples of the boomerang represent mixing between the two cooling end members, as indicated by their annealed, bimodal MTLs with large standard deviations (circle size).

Figure 5: Map showing (a) regional AFT MTL and (b) age data modified from Kohn et al. (2002) and Gleadow et al. (2002b) interpolated between points using a continuous spline in tension, overlying DEM and bathymetry maps. Data from this study is not included in the figure as it largely follows the same trend as previous studies in the area and would not markedly affect the output at the given resolution. The axis of the boomerang trend (dashed yellow line), edge of the Great Escarpment lip (white trace), location of transect for this study (white rectangle), data locations (white dots), and outline of extent of present-day Sydney basin (black trace, shaded white) are shown.

Figure 6: Inverse thermal history models generated from HeFTy software, v. 1.8 (Ketcham et al., 2005). Ketcham et al. (2007a) and Ketcham et al. (2007b) were used as c-axis projection and annealing models (5M) respectively. Dpar was used as the kinetic parameter, allowing for initial MTL from Dpar measurements. Comparison between modeled and observed AFT data for best-fit model paths accompany each thermal history shown above. Model reproducibility of the observed track length histograms are shown in the bottom right corner of each thermal history. Samples were allowed to re-heat between constraints, as indicated in the figure, i.e.: 3Ev—3 halves, episodic variable. Models were allowed to run until 100 "good" ($p>0.5$) paths were found to fit the model. Present-day surface temperature was set at 20±10°C. Model paths have been cropped above 140°C, far outside the apatite PAZ. An initial constraint was added to start the model, which was well out of the partial annealing zone ages much older than the AFT age. A broad constraint was also used for samples 12 and 13 to allow for the possibility of cooling/reheating between the initial constraint and AHe age, this constraint never truncated the model and only served to allow more flexibility between the starting and ending constraints. Furthermore, in some instances the AHe age range (highlighted purple) was used as a constraint (MM14-12, 13, 18B, 20), however in every instance (except MM14-18B; robust undispersed age) the constraint was only used as a guide, and was adjusted/enlarged if the model truncated on the border of the constraint. Extra models, including "wide-open" constraints for MM14-12 and MM14-13 can be found in the Supplementary Information.

Table 1

Summary of Apatite Fission Track (AFT) Results

Sample No.	Map ID	Map Unit	Rock Type	Longitude/Latitude	Elevation [m]	No. of grains	N_s	ρ_s [10^5 cm^{-2}]	^{238}U [ppm ± 1σ]†	D_{par} [µm]	Dispersion [%]	Pooled age [Ma ± 1σ]	Central age [Ma ± 1σ]	N_{length}	Mean track length [µm ± se]	St.Dev. [µm]†
Zone 1:																
MM14-01	Dggg	Glenbog Granodiorite	Granodiorite	149.31044/-36.57578	1074	25	1456	26.2504	20.4 ± 11.4	1.38	19	261 ± 16	288 ± 15	107	13.16 ± 0.06	0.66
MM14-02	Dggn	Minnitabel Adamellite	Biotite Adamellite	149.34836/-36.60051	1130	30	2528	38.4000	31.9 ± 19.9	1.35	30	252 ± 20	273 ± 17	100	12.79 ± 0.08	0.77
MM14-03	Dgbb	Bemboka Granodiorite	Granodiorite	149.40134/-36.61925	1108	33	656	7.6167	6.3 ± 1.8	2.25	0	256 ± 10	261 ± 11	98	12.75 ± 0.10	0.98
MM14-04	Dgbb	Bemboka Granodiorite	Granodiorite	149.44353/-36.59805	893	31	521	7.3490	6.2 ± 2.8	1.6	19	242 ± 16	258 ± 15	90	12.47 ± 0.11	1.03
MM14-05	Dgbb	Bemboka Granodiorite	Granodiorite	149.45609/-36.60470	709	29	422	5.6349	5.0 ± 1.4	1.44	16	234 ± 16	242 ± 15	101	12.44 ± 0.11	1.15
MM14-06	Dgbb	Bemboka Granodiorite	Granodiorite	149.46900/-36.61010	515	30	461	7.2774	6.4 ± 1.8	1.46	8	245 ± 13	251 ± 14	100	11.66 ± 0.15	1.46
Zone 2:																
MM14-07	Dgbb	Bemboka Granodiorite	Granodiorite	149.48102/-36.60967	374	28	427	6.0364	5.5 ± 1.6	1.49	0	234 ± 11	239 ± 12	120	11.30 ± 0.20	2.19
MM14-08	Dgbb	Bemboka Granodiorite	Granodiorite	149.51382/-36.61748	240	31	524	6.0742	5.9 ± 1.7	1.54	11	213 ± 13	220 ± 11	113	11.60 ± 0.16	1.69
MM14-09	Dgbb	Bemboka Granodiorite	Granodiorite	149.57607/-36.63217	212	31	361	5.0415	5.6 ± 2.1	1.57	5	193 ± 14	199 ± 11	125	11.31 ± 0.16	1.81
MM14-10	Dgbb	Bemboka Granodiorite	Granodiorite	149.62241/-36.66134	176	25	370	6.0940	6.7 ± 2.7	1.6	0	201 ± 9	203 ± 11	109	11.13 ± 0.20	2.07
MM14-11	Dgbb	Bemboka Granodiorite	Granodiorite	149.62456/-36.66122	175	29	424	5.4642	6.0 ± 2.3	1.45	0	194 ± 9	199 ± 10	109	11.13 ± 0.15	1.55
MM14-12	Dgrb	Brogo Granodiorite	Granodiorite	149.85004/-36.63938	47	29	1900	14.5260	20.5 ± 7.6	1.47	9	156 ± 5	154 ± 5	115	11.65 ± 0.25	2.72
MM14-13	Dgkk	Kameruka Granodiorite	Granodiorite	149.77303/-36.63703	209	32	921	8.2975	9.7 ± 3.8	1.59	16	179 ± 9	183 ± 8	115	9.84 ± 0.26	2.81
MM14-14	Dgbb	Bemboka Granodiorite	Granodiorite	149.71213/-36.62487	130	28	1665	26.2119	33.3 ± 16.4	1.18	11	171 ± 7	169 ± 6	106	9.56 ± 0.25	2.60
MM14-15	Dgrb	Brogo Granodiorite	Granodiorite	149.82296/-36.56382	60	30	508	8.2857	12.2 ± 4.5	1.5	15	145 ± 9	149 ± 8	110	10.92 ± 0.23	2.39
MM14-16	Dgrb	Brogo Granodiorite	Granodiorite	149.82284/-36.56389	62	33	169	1.2597	1.7 ± 0.2	1.9	0	163 ± 6	166 ± 13	94	10.90 ± 0.21	2.08
MM14-24	Dgrb	Brogo Granodiorite	Granodiorite	149.86678/-36.71383	12	30	1826	17.1710	26.7 ± 9.4	1.65	17	140 ± 6	139 ± 6	113	12.20 ± 0.18	1.88
Zone 3:																
MM14-17	Oa	Adaminaby Group	Sandstone	150.05594/-36.49609	2	31	456	6.5367	20.0 ± 17.9	1.35	6	70 ± 5	73 ± 4			
MM14-18A	Dgug	Goalen Head Gabbro	Gabbro	150.06191/-36.55727	3	33	173	1.8337	3.5 ± 0.8	1.53	0	107 ± 8	114 ± 9	87	13.75 ± 0.10	1.00
MM14-18B	Dgug	Goalen Head Gabbro	Pegmatite	150.06191/-36.55727	3	33	163	1.1836	2.6 ± 0.4	1.38	0	94 ± 9	103 ± 9	97	13.80 ± 0.09	0.93
MM14-19	Dbb	Boyd Volcanic Complex	Quartzite	150.03031/-36.56682	112											
MM14-20	Kts	Tanja Syenite	Syenite	149.98955/-36.62984	48	38	452	4.7472	11.3 ± 8.8	1.56	21	93 ± 8	97 ± 6	97	13.84 ± 0.13	1.27
MM14-21	Oa	Adaminaby Group	Sandstone	150.01481/-36.64506	2	23	1207	9.3085	23.5 ± 20.7	1.92	31	87 ± 7	85 ± 7	52	13.66 ± 0.12	0.83
MM14-22	Dgld	Dr. George Granite	Leucogranite	149.92633/-36.65046	149	29	128	2.3266	19.7 ± 18.6	1.43	149	20 ± 23	37 ± 11	29	13.79 ± 0.14	0.79
MM14-23	Dgld	Dr. George Granite	Leucogranite	149.90569/-36.66819	260	6	116	5.4724	13.1 ± 10.3	1.22	86	125 ± 53	71 ± 28			
MM14-25	Dba	Boyd Volcanic Complex	Porphyritic Rhyolite	149.99081/-36.72646	20	6	39	3.0912	8.4 ± 4.9	1.64	0	80 ± 11	83 ± 14			

Analyses were performed on image sets captured by *TrackWorks* using a 4.0MP *IDS uEye UI-3370CP-C-HQ* camera mounted on a *Zeiss AxioImager* microscope with a 1000x total magnification and a 100x dry objective (calibration = 0.087/0.087µm/pixel). Spontaneous track densities were measured on prismatic internal apatite surfaces after etching with 5M HNO_3 for 20sec at 20ºC. Track counts were obtained by automated counting in *FastTracks* using the 'coincidence mapping' technique of Gleadow et al. (2009) followed by manual inspection. Uranium concentrations of each grain were determined by LA-ICP-MS single spot analysis using a *New Wave* Nd:YAG Laser (λ=213nm with 5Hz @ 45% power, spot size=30µm) connected to an *Agilent 7700* mass spectrometer. NIST612 was used as an internal LA-ICP-MS standard. Single grain and pooled ages were calculated according to Hasebe et al. (2004) using an 'aggregate constant' of 2010 (2.007 ± 0.007 X 10-3), equivalent to a zeta calibration. Central ages were estimated from single grain ages and errors according to the formulas given by Galbraith (2005, p.100) using the Newton-Raphson method. All ages are "model" ages obtained using a range factor (Rs) of 7.17µm (average mean track length of Durango and Fish Canyon Tuff standards) and are directly comparable to conventional External Detector Method ages (Seiler et al., 2014). Confined track lengths (TINTs) were measured as true 3D lengths using *FastTracks* after irradiation by ^{252}Cf and etching with 5M HNO_3 for 20sec at 20ºC. Track lengths are corrected for a refractive index of 1.634 for apatite. For a more comprehensive expalaination of AFT methodology see Gleadow (2015).

† Standard deviation of mean

N_s = number of spontaneous tracks counted; ρ_s = spontaneous track density; D_{par} = long axis of track etch pit; N_{length} = number of lengths measured; se = standard error

Table 2
Summary of Single Grain Apatite (U-Th-Sm)/He Data

Sample	Lab. No.	He#	^{4}He (ncc)	Mass (mg)	[a]Mean F_T	U ppm	Th ppm	Sm ppm	Th/U	[b][eU] ppm	Uncorrected Age (Ma)	Age [Ma ± 1σ]	Grain length (μm)	Grain radius (μm)	[c]R_s (μm)	[d]Grain morphology
MM14-5	11523	35980	0.432	0.0029	0.70	7.3	22.6	458.6	3.09	12.6	92.6	133 ± 8	189.5	46.9	56.4	1T
MM14-5	11524	35983	1.603	0.0077	0.76	7.9	38.3	371.1	4.84	16.9	98.3	129 ± 8	238.4	56.5	68.5	0T
											Central age	131 ± 6				
MM14-10	11526	35991	0.404	0.0057	0.73	3.6	13.3	256.7	3.67	6.7	82.2	113 ± 7	258.2	46.8	59.4	0T
MM14-10	11527	36075	0.489	0.0038	0.73	5.8	22.2	407.5	3.84	11.0	92.1	127 ± 8	198.5	52.7	62.5	1T
MM14-10	11528	36078	0.475	0.0058	0.75	4.4	13.6	251.6	3.07	7.6	83.6	112 ± 7	204.8	53.2	63.4	0T
MM14-10	*11529*	*36081*	*0.430*	*0.0034*	*0.71*	*8.3*	*30.5*	*491.4*	*3.69*	*15.5*	*65.3*	***92 ± 6***	*194.6*	*50.1*	*59.7*	*1T*
											Central age	117 ± 4				
MM14-12	11530	36084	1.333	0.0057	0.74	21.4	37.3	127.0	1.74	30.2	62.7	84 ± 5	228.2	50.0	61.5	0T
MM14-12	11531	36087	1.809	0.0108	0.80	15.3	32.4	152.9	2.12	22.9	59.3	**74 ± 5**	199.6	73.4	80.5	0T
MM14-12	11532	36090	1.942	0.0090	0.79	14.3	30.6	142.2	2.14	21.5	81.7	103 ± 6	187.6	69.0	75.6	0T
MM14-12	11533	36093	1.095	0.0038	0.74	23.0	42.0	242.6	1.83	32.9	71.3	96 ± 6	178.1	57.0	64.8	1T
											Central age	93 ± 7				
MM14-13	11534	36096	2.940	0.0108	0.79	14.6	26.8	286.8	1.83	20.9	104.6	**132 ± 8**	303.0	59.5	74.6	0T
MM14-13	11535	36099	1.913	0.0096	0.78	15.7	34.8	322.7	2.22	23.9	66.9	**86 ± 5**	291.6	57.3	71.8	0T
MM14-13	11536	36102	3.750	0.0081	0.80	29.3	49.0	488.1	1.67	40.8	91.2	**114 ± 7**	224.9	74.6	84.0	1T
											Central age	**Dispersed**				
MM14-18B	11545	36108	0.386	0.0059	0.76	4.4	10.9	358.9	2.48	7.0	72.6	95 ± 6	236.9	59.9	71.7	1T
MM14-18B	11546	36111	0.272	0.0086	0.76	2.0	5.8	233.1	2.87	3.4	70.0	92 ± 6	299.1	53.6	68.1	0T
MM14-18B	11548	36117	0.411	0.0125	0.79	2.1	5.6	215.6	2.64	3.4	72.7	92 ± 6	368.9	58.1	75.3	0T
											Central age	93 ± 3				
MM14-20	11549	36120	1.491	0.0110	0.78	7.8	39.6	104.5	5.07	17.1	64.2	83 ± 5	301.7	66.3	81.5	2T
MM14-20	11550	36123	1.072	0.0077	0.76	7.3	38.8	101.0	5.32	16.4	68.9	91 ± 6	221.5	64.6	75.0	2T
MM14-20	*11551*	*36126*	*0.347*	*0.0085*	*0.77*	*3.5*	*15.3*	*66.4*	*4.35*	*7.1*	*46.4*	***61 ± 4***	*230.1*	*66.7*	*77.6*	*2T*
MM14-20	11552	36129	1.248	0.0106	0.80	6.0	37.0	137.1	6.20	14.7	65.1	81 ± 5	291.8	72.2	86.8	1T
											Central age	85 ± 3				
MM14-24	11553	36132	1.102	0.0099	0.79	14.6	34.3	154.7	2.34	22.7	39.7	**50 ± 3**	223.4	66.5	76.9	0T
MM14-24	11555	36138	2.262	0.0122	0.80	20.7	40.5	212.4	1.96	30.2	49.9	**62 ± 4**	357.7	68.5	86.3	1T
MM14-24	11556	36141	5.063	0.0182	0.82	14.0	32.3	205.7	2.30	21.6	103.5	**126 ± 8**	340.1	73.0	90.2	0T
											Central age	**Dispersed**				

Results from 7 samples selected based on euhedral grain geometry and relatively equal spacing from one another along transect. Apatite were hand picked; only clear, euhedral grains were selected for analysis, however, the terminations of apatite grains may or may not have been intact, as noted above. Grains were then placed in ethanol and checked for inclusions under polarized light. Grain geometries were imaged and measured in order to apply the α-ejection correction. The apatites were then placed in a Pt capsule and outgassed under vacuum at 900 °C for 5 min using a fibre-optically coupled Coherent Quattro FAP 820 nm diode laser. ^{4}He content was the measured by isotope dilution using a pure ^{3}He spike, measured using a Balzers Prisma QMS 200 quadrupole mass spectrometer and calibrated against and independent ^{4}He standard. The degassed apatites were then dissolved in their capsules using HNO_3 for analysis of ^{238}U, ^{235}U, ^{232}Th and ^{147}Sm. Samples were calibrated against reference material BHVO-1, with recrystallized homogenized Mud Tank Carbonatite apatite, Durango apatite and rock standard BCR-2 were used as internal standards. Alpha-ejection was calculated following Farley et al. (1996). Analytical uncertainties at the University of Melbourne He facility have been estimated to be ~6.2%. This includes the α-ejection correction, a 5 μm grain dimension uncertainty, gas and ICP-MS analytical uncertainties, but does not included the possibility of lattice heterogeneity. Accuracy of U, Th and Sm content is typically better than 1% (Jiao et al., 2014; Gleadow et al., 2015).

Central ages were calculated following Vermeesch (2008). Ages in ***bold*** were considered overly dispersed an not used in central age calculations.

[a]F_T = α-ejection correction after Farley et al. (1996)

[b]Effective uranium content [U ppm + 0.235*Th ppm]

[c]R_s = equivalent sphere radius of the crystal.

[d]Grain morphology - 0T = no crystal terminations, 1T = one crystal termination and 2T = 2 crystal terminations.

Table 3

Summary of effective elastic thickness (T_e) estimations dervied from AFT data

Sample	Elevation	[a]T_{max} during rifting (T_r)	Assumed geothermal gradient (G)	[b]Total exhumation (ΔE) since rifting	[c]Effective elastic thickness (T_e)	[d]Natural flexural lithospheric wavelength (w_c)	Flexural rigidity of the lithosphere (D)	[e]Isostatically driven exhumation [$h_i(T_e)$]	Total exhumation [$\Delta E(T_e)$]
	(m)	°C	°C/km	km	km	km	pa*km^3	km	km
MM14-18B	3	120	25	4 (min.)	0	0	0	7.5	9
					1	4.3	8.889E+15	6.3	7.8
					2.16[†]	**7.6**	**8.973E+16**	**2.5**	**4**
					2.5	8.5	1.389E+17	1.8	3.3
					5	14.2	1.111E+18	0.3	1.8
					10	24	8.889E+18	0.04	1.54
					15	32.4	3.000E+19	0.01	1.51

Values for total denudation as a function of T_e were calculated using increasing values of T_e with an initial h_0 value (estimated as the height of eroded escarpment ~1.5 km). Isostatically driven exhumation (h_i) was then calculated as described below (e). To calculate the **bolded** best-fit case to the given AFT data (assuming ΔE = 4km[b]), D was estimated as a function of h_i and h_0 from a given h_0 and ΔE where $D = [(h_0/h_i+1-\rho_m/\rho_c)/(2pi/\lambda)4]\rho_c g$, where p_m and p_c are the densities of mantle and crust respectively (3300 kg m^{-3} and 2750 kg m^{-3} in this case), λ = wavelength, taken as the width of the coastal plain (60 km in this case). Effective elastic thickness (T_e) was then estimated from D; where $T_e=[(12(1-v2)D)/Y]^{1/3}$ where v = Poisson's ratio (0.25), Y = Young's modulus (10^{11}Pa) (Braun and van der Beek, 2004, and references within).

[†] **Bolded** scenario represents the calcualted T_e value to fit the given data derived from AFT ages along the coastal plain as described above.

[a] Rifting is assumed to commence ~110 Ma. Sample MM14-18B T_{max} was greater than the PAZ T range (~60-120°C), therefore the T_{max} value of 120 was used.

[b] Total exhumation (ΔE) = $[(T_r - T_s)/G](k)$ where $T_r = T_{max}$ at time of rifting dervied from *HeFTy* (Ketcham, 2005) thermal history models, T_s = mean annual surface T (20°C in this case), G = assumed geothermal gradient and k = thermal conductivity ratio of denuded rock to the remaining section (1 in this case) (Brown, 1991).

[c] Effective elastic thickness (T_e) was input in all cases except the bolded case as described above.

[d] $w_c = (D/\rho_c g)^{1/4}$ Where denudation taking place when $\lambda << w_c$ will not be accompanied by significant isostatic rebound (i.e. plate deflection is negligible when compared to amplitude of the topography) and when $\lambda >> w_c$ will be isostatically compensated (i.e. the lateral strength of the lithosphere becomes negligible when considering wide loads and the topography trends towards isostatic equilibrium, resulting in Airy isostasy when $T_e = 0$ $\therefore$ $h_i = h_0/(\rho_m/\rho_c-1)$ (Walcott, 1970; Turcotte and Schubert, 1982; Braun and van der Beek, 2004).

[e] Isostatically driven exhumation was allowed to vary in all cases (except bolded case) given an initial eroded escarpment height (h_0) and T_e where $h_i = h_0/[(\rho_m/\rho_c)-1+(D/\rho_c g)(2pi/\lambda)^4]$ and $D = YT_e^3/[12(1-v^2)]$) (Turcotte, 1979; Turcotte and Schubert, 1982; Braun and van der Beek, 2004).

Note: increasing the eroded escarpment height (h_0), wavelength (λ), and geothermal gradient (G), which effectively lessens the amount of total exhumation required (ΔE), allows for thicker effective elastic thickness estimations (T_e). Values used above were considered conservative and/or nominal. i.e.: Using G = 40°C/km, ΔE = 2.5km h_0 = 2km, λ = 150km allows for a more reasonable T_e = 15km (e.g. Zuber et al., 1989). Of these variables, the paleo-geothermal gradient estimation is the greatest unknown.

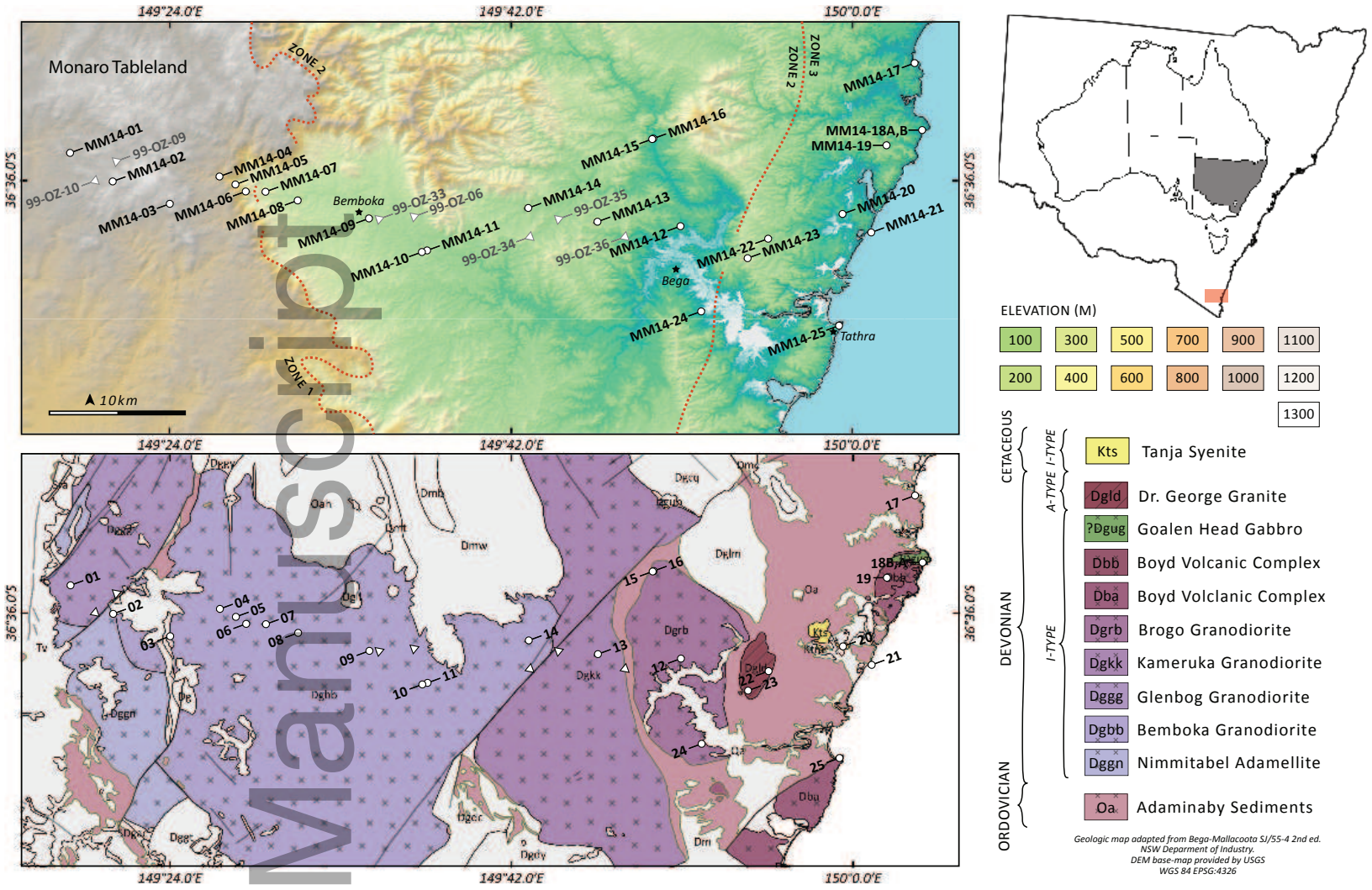

ter_12441_f1.eps

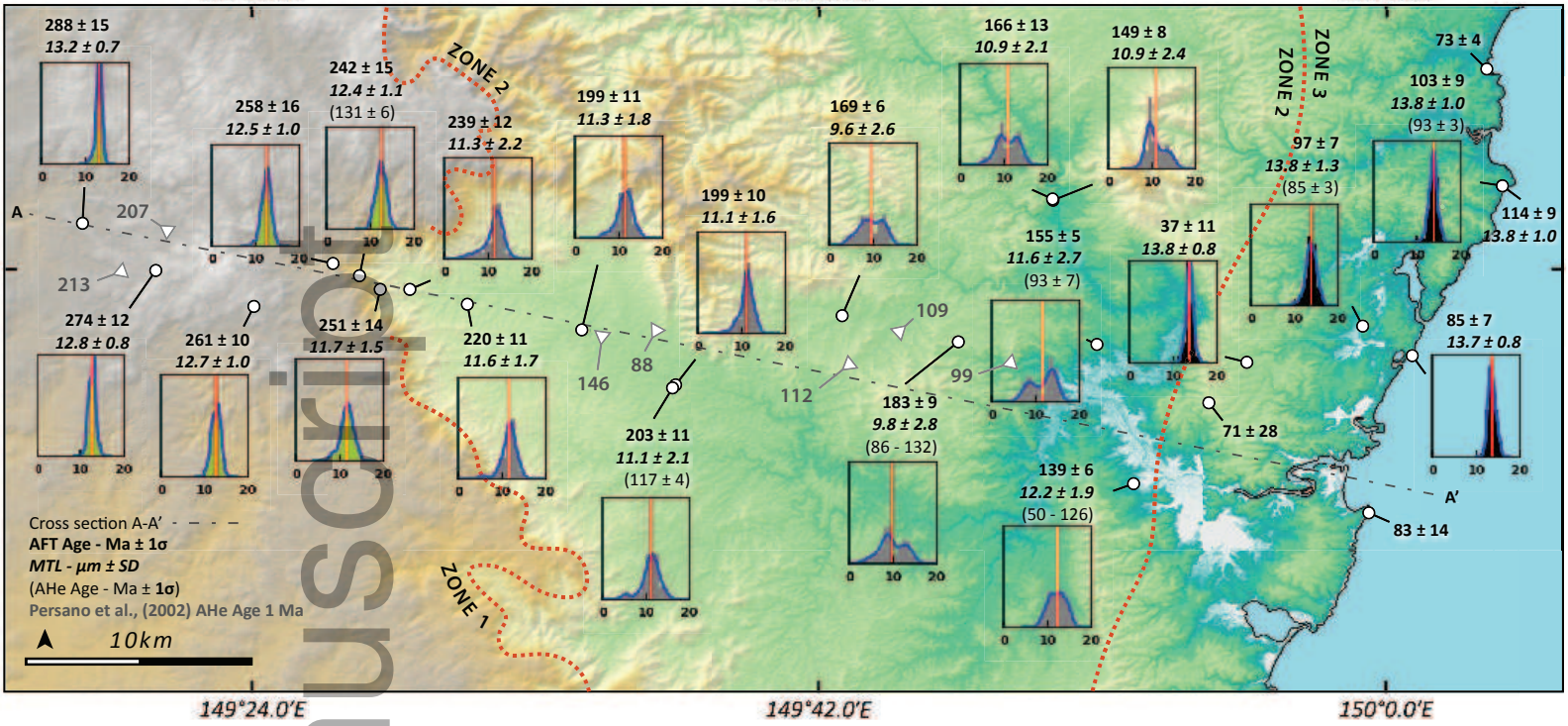

ter_12441_f2.eps

Fission track (Ma ± 1σ) and AHe age *(Ma ± 1σ)* across cross section A-A'

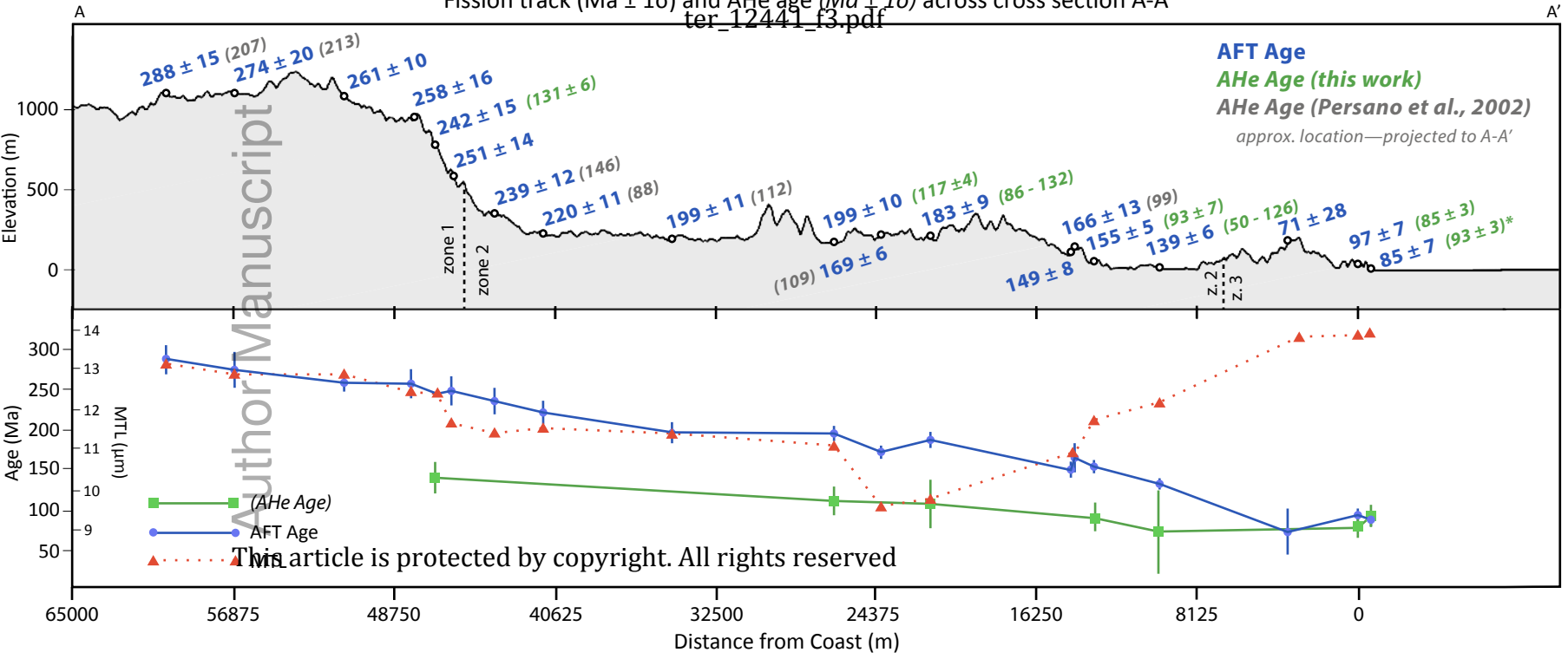

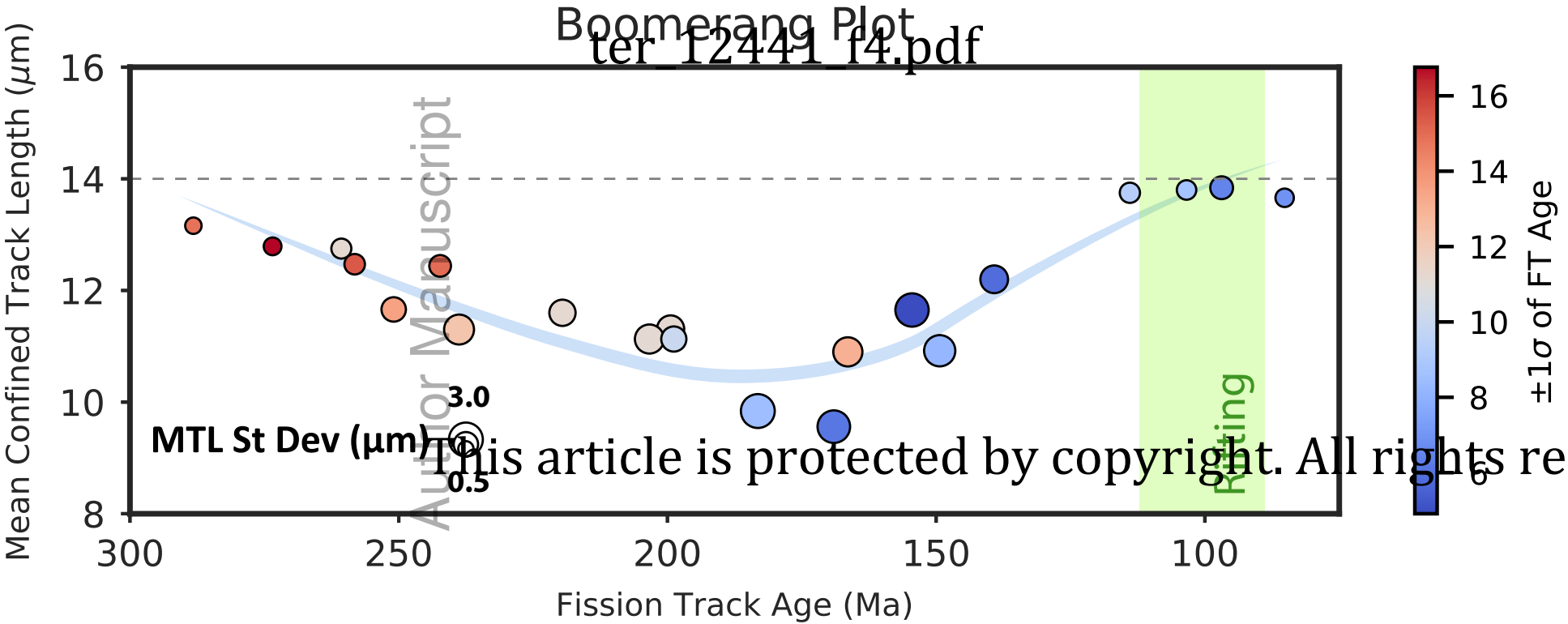

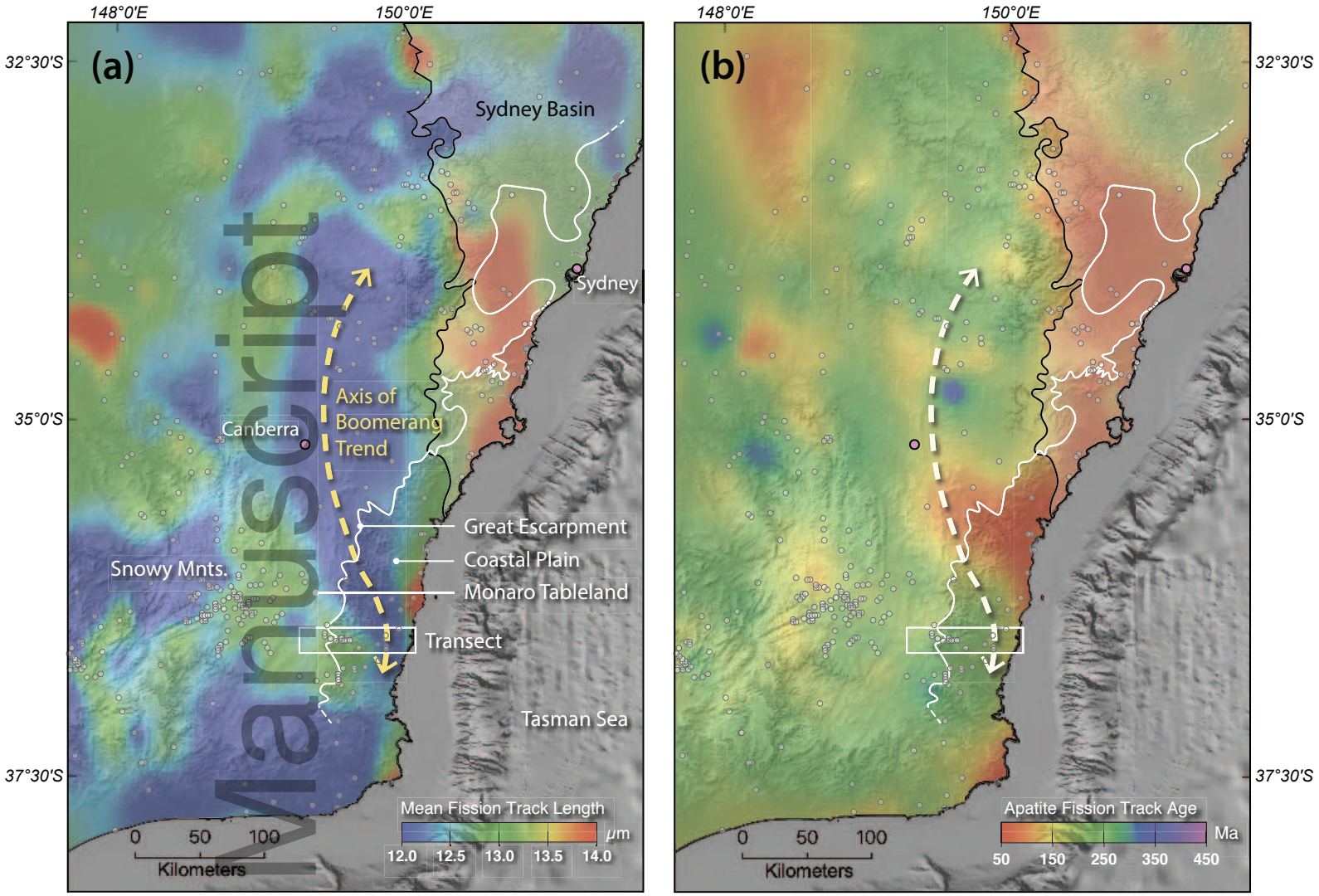

ter_12441_f5.eps

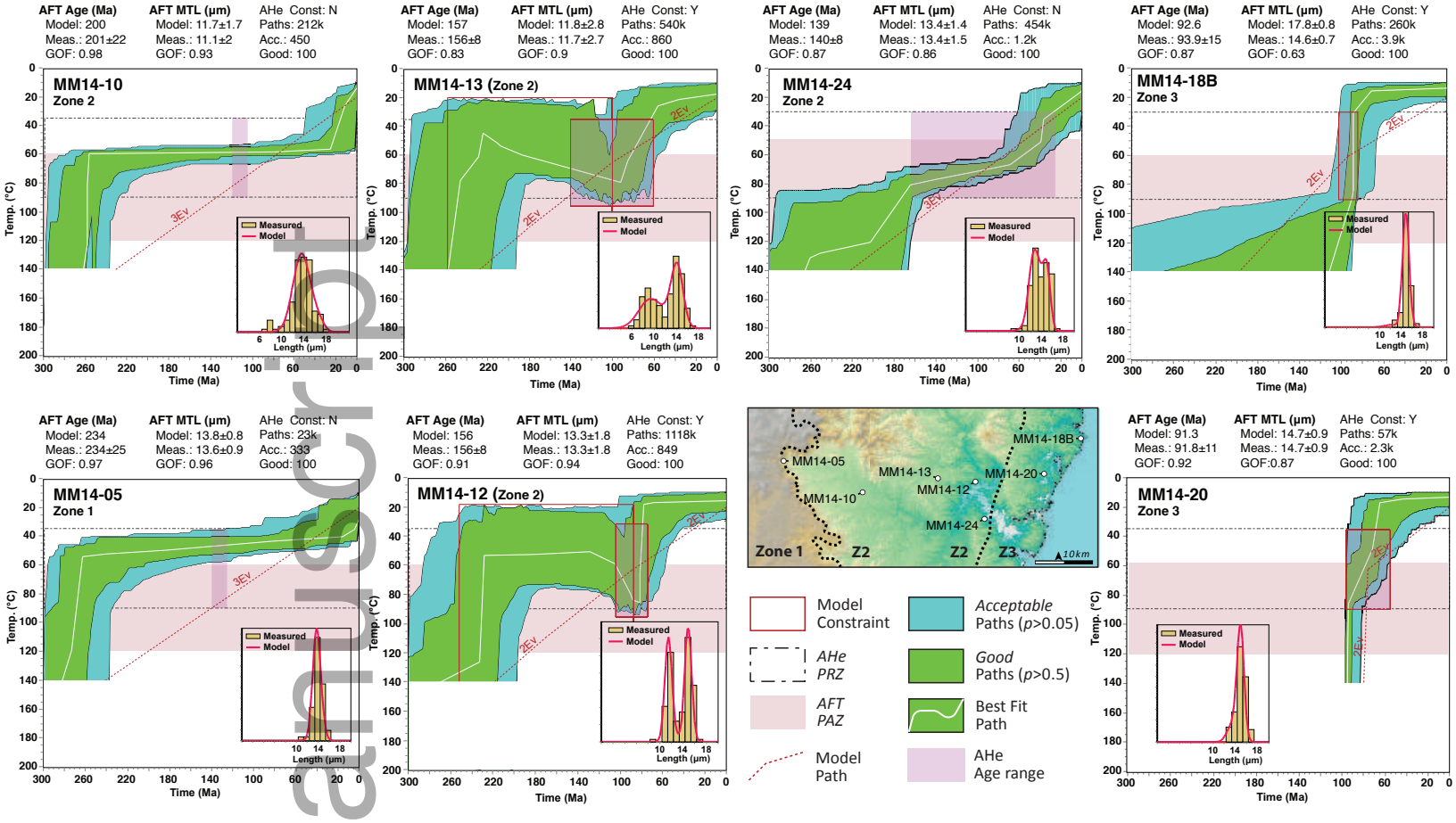

ter_12441_f6.eps